Supporting Information

Microstructural Response of Variably Hydrated Ca-rich Montmorillonite to Supercritical CO_2

Mal-Soon Lee[a], *B. Peter McGrail*[b], *Vassiliki-Alexandra Glezakou*[a]*

[a]Fundamental and Computational Sciences, [b]Energy and Environment,
Pacific Northwest National Laboratory, Richland, WA 99352.

Corresponding Author: Vanda.Glezakou@pnnl.gov

Contents

Computational Details. We employed DFT-based molecular dynamics simulations within the generalized gradient approximation (GGA) with the exchange correlation functional of Perdew, Burke and Ernzerhoff (PBE)[1] as implemented in the CP2K package[2-3]. Dispersion corrections were taken into account using Grimme's et al. third-generation corrections (DFT-D3) as described in their recent paper[4]. The C(6) coefficients in this newer scheme have been shown to yield much more accurate energies for adsorption processes on ionic surfaces[5]. The core electrons in our systems were described by norm-conserving pseudopotentials[6-7], while the valence wave function was expanded in terms of double-zeta quality basis sets optimized for condensed systems to minimize linear dependencies and superposition errors[8]. An additional auxiliary plane-wave basis set with a 500-Ry cutoff was used for the calculation of the electrostatic terms[9]. The Γ-point approximation employed for the Brillouin zone integration was deemed appropriate because of the significant size of the supercell, as described below.

As a starting point for our models, we used the 2:1 dioctahedral aluminous Ca-rich smectite with the chemical formula $Al_2Si_4O_{12}Ca_{0.5}$ used by Vianni et al. to study the nature of disorder in montmorillonites[10]. The majority of density functional calculations we encountered in the literature use only one intercalated cation per unit cell. To study the effect of co-existing Ca ions in the interlayer spacing, we chose not to substitute any of the octahedral Al with Mg. However, we tested the effect of interlayer substitution (by Mg) but found no significant changes to the cell parameters. The resulting 2×1×1 supercell used in our simulations contained two interlayer Ca ions and $4H^+$ within the clay layer. The initial lattice parameters of the supercell were adopted from the work of

Berghout et al.[11], *a*=10.48 Å, *b*=9.03 Å, *c*=10.06 Å, *a*=90.9º, *b*=99.3º, and *g*=90º, who optimized the cell parameters of various montmorillonites.

We examined an array of systems by varying the number of interlayer H_2O and CO_2 molecules, ranging from 0, 4, 6, 8, and 10H_2O, and 0, 2, and 4CO_2. The system 6H_2O-4CO_2 was also modified to include SO_2 as 6H_2O-3CO_2-SO_2. For each system, the supercell parameters as well as the atomic positions were fully optimized at *P*=90 bar, which was one of the experimental parameters used by our collaborators[12]. To determine the local structure, atomic density distributions, and various thermodynamic properties under experimental conditions, we performed DFT-based molecular dynamics simulations within the canonical *NVT* ensemble at *T*=323 K, the temperature used in the experimental studies by Schaef et al.[12]. The simulations were initiated with structures obtained by the cell optimizations at 90 bar using a 0.5-fs time step. The temperature was controlled by a Nose-Hoover chain thermostat with a frequency of 4000 cm^{-1}. To check the validity of the *NVT* ensemble, ab initio molecular dynamics (AIMD) simulations with the isobaric-isothermal ensemble (*NPT)* at the experimental conditions of *P*=90 bar and *T*=323 K for selected systems were also performed. Subsequent analysis from both approaches gave similar statistical properties; however, the *NPT* simulations were very time-consuming and it would be impossible to apply them for all the systems examined at the significant timescales required to accumulate reliable statistics, particularly the IR spectra. Because the results were consistent, the analysis presented below is from trajectories in the canonical ensemble, while monitoring the stress tensor to maintain the target pressure.

Trajectories were initially equilibrated by means of a thermostat for about 5 ps, followed by canonical runs of 20-25 ps. Statistical averages were typically collected in the last 15-20 ps of the simulation by examining the convergence of the statistics with different time intervals. The following properties were calculated:

(a) Density profiles of the interlayer species along the z direction, showing the distribution of each species with respect to the mid-plane parallel to the clay layers.

(b) Pair distribution functions representing the average distance of any two atomic species a and β:

$$g_{\alpha\beta}(r) = \frac{1}{N_\alpha \rho_\beta} \sum_{I\epsilon\alpha, J\epsilon\beta} \delta(r - |\boldsymbol{R}_J - \boldsymbol{R}_I|),$$

where ρ_β is the average density of atoms of species β and N_α corresponds to the number of atoms of species α. Integration of this function gives the coordination number of species β around α.

(c) X-ray diffraction (XRD) spectra were calculated from:

$$S_{\alpha\beta}(\vec{q}) = \frac{1}{N_\alpha f_\alpha(q)^2 + N_\beta f_\beta(q)^2} \langle \sum_j f_j(q) \exp(i\vec{q} \cdot \boldsymbol{R}_j) \sum_k f_k(q) \exp(i\vec{q} \cdot \boldsymbol{R}_k) \rangle,$$

where $\boldsymbol{R}_j$, $\boldsymbol{R}_k$ denote the position of atoms j and k, N is the total number of atoms of species, while the thermal averages (in brackets) are taken over the molecular dynamics trajectory[13]. The atomic form factors were approximated by the general expression

$$f(s) = \sum_{n=1}^{4} a_n \exp(-b_n s^2) + c,$$

where $s = \sin\theta/\lambda = q/4\pi$. The parameters a_n, b_n, and c for each species were adopted from published data[14].

(d) Infrared (IR) spectra were calculated from the Fourier transform of the autocorrelation of the total dipole moment. The harmonic approximation was used to extract the quantum correction factor that satisfies the fluctuation-dissipation theorem[15]. The resulting absorption coefficient is defined as:

$$\alpha(\omega) \propto \omega^2\beta \int_{-\infty}^{+\infty} dt e^{-i\omega t}\langle \boldsymbol{M}(t)\cdot\boldsymbol{M}(0)\rangle,$$

where T is temperature, $\beta=(k_BT)^{-1}$, $\boldsymbol{M}$ is the total dipole moment, and the angular brackets indicate the statistical average over time. The total dipole moment at each time step was evaluated using the Berry-phase approach[16]. In addition, we calculated the vibrational density of states projected on each species using velocity autocorrelation function to assign the contribution of different species to the spectra.

(e) To study the relative stability at 323 K, we calculated their free-energy difference (ΔF) using $\Delta F=\Delta E(T) - T\Delta S$, where $\Delta E(T)$ is the average energy difference at T and ΔS is the entropy difference between them. The entropy difference was obtained using a VDOS approach[17-18]

$$S = 3k_B \int_0^{\infty} D(\omega)\left\{\frac{\hbar\omega}{2k_BT}\coth\left(\frac{\hbar\omega}{2k_BT}\right) - \log\left[2\sinh\left(\frac{\hbar\omega}{2k_BT}\right)\right]\right\} d\omega$$

where $D(\omega)$ is the vibrational density of states obtained from velocity autocorrelation.

(f) Diffusion coefficients along the clay surface, $D_{\parallel}$, were calculated using the two-dimensional Einstein relation:

$$D_{\parallel} = \lim_{t\to\infty} \frac{\langle \Delta x(t)^2 + \Delta y(t)^2 \rangle}{4t}$$

where the $<\Delta x(t)^2+\Delta y(t)^2>$ is the mean square displacement of the particle along the *xy* plane.

Cell Optimizations. In the undersaturated environments, one of the calcium atoms gravitated towards the clay surface regardless of the starting geometries. We consider 4-6H_2O interlayer waters to be fair approximations for undersaturated systems up to 1W hydration level[11]. The final geometries of the dry and water-only systems are shown in Figure S1, and with both H_2O and CO_2 in Figure S2. The optimized cell parameters, supercell volume, and corresponding d_{001} spacing are summarized in Table S1. For certain systems, the cell optimization was performed at additional pressures, other than 90 bar, but there was almost no discernible difference in the *d*-spacing. This is consistent with experimental work showing that hydrated clays are fairly stable under a wide range of pressures.

In the extreme, idealized "dry" system, one of the interlayer Calcium atoms ends up on the clay surface over the hexagonal Si-ring, while the remaining cation still stays approximately at the middle of the interlayer space, as shown in Figure S1(a). The clay layer, unsurprisingly, undergoes severe contraction, with the interlayer space being reduced to ~2.7 Å. Introduction of water in the interlayer space, Figure S1 (b) with 4H_2O and Figure S1(c) with 6H_2O, causes expansion of the space by ~19-20% as can be

inferred by the measured d_{001}-spacings. Although the clay layer expands slightly, the expansion comes mainly from the interlayer space. Regardless of their positions, both Ca ions maintain ~5-6 coordination contacts (within ~2.7 Å) with nearby water and/or surface oxygens. The calcium in the interlayer space remains in the mid-plane along with the coordinating waters.

Table S1. Simulation cell optimized parameters for a smectite model with two interlayer Ca cations, $(Al_4Si_8O_{22})_2(OH)_4Ca_2$:$(H_2O)_n$-$(CO_2)_m$, with n=0, 4, 6 and m=0, 2, 4.

Model system		*a*	*b*	*c*	*α*	*β*	*γ*	V(Å^3)	d_{001}
***m*=0**	***n*=0**	10.44	9.01	9.55	82.2	98.2	89.9	880.6	9.37[a,b]
***m*=0**	***n*=4**	10.39	8.99	11.28	87.6	98.3	89.4	1041.4	11.15[a,b]
	***n*=6**	10.38	9.00	11.43	88.0	98.7	89.5	1054.1	11.29[a,b]
***m*=2**	***n*=4**	10.44	9.00	12.14	89.5	98.7	90.0	1125.76	12.00
	***n*=6**	10.45	9.03	12.36	89.5	98.4	89.3	1153.47	12.23
***m*=4**	***n*=4**	10.40	9.02	12.14	90.0	98.5	89.6	1125.76	12.01
	***n*=6**	10.43	9.05	12.80	91.0	99.0	89.4	1194.30	12.65

[a]Experimental d_{001}values for Ca^{2+} montmorillonite are 9.55-10.3 Å for dry[19-23] and 11.19-12.85 for 1L systems[20-22, 24]. [b]d_{001} values from DFT calculations 9.93, 11.96, 12.31 Å for n=0, 4 and 6 respectively[11] and 9.98 and 11.33Å for n=0 and 2[25].

Table S2. Cell optimized parameters for a smectite model with two interlayer Ca cations, $(Al_4Si_8O_{22})_2(OH)_4Ca_2$:$(H_2O)_n$-$(CO_2)_m$, with n=8, 10 and m=0, 2, 4.

Model system		*a*	*b*	*c*	*α*	*β*	*γ*	V(Å^3)	d_{001}
***m*=0**	***n*=8 (2W)**	10.37	8.98	14.13	89.6	94.6	89.9	1313.20	14.10[a]
	***n*=10 (2W)**	10.37	8.97	14.24	90.2	93.2	90.0	1322.77	14.22
***m*=2**	***n*=8 (Q-1W)**	10.38	8.98	13.11	86.9	95.4	88.6	1214.72	13.03
	***n*=10 (Q-1W)**	10.35	8.92	13.30	85.5	95.1	87.9	1216.88	13.20
	***n*=10 (2W)**	10.38	8.98	14.12	90.2	93.5	89.9	1313.05	14.10
***m*=4**	***n*=8 (Q-1W)**	10.39	8.95	13.25	86.7	95.0	88.8	1226.10	13.18
	***n*=10 (Q-1W)**	10.36	8.95	13.48	85.7	95.4	87.6	1125.76	13.38
	***n*=10 (2W)**	10.37	8.98	14.22	89.9	93.5	90.0	1194.30	14.20

[a]Experimental d_{001}values for Ca^{2+} montmorillonite in 2L are 14.30-15.81 Å[19-22, 24]. From DFT calculations 2L (with $6H_2O$) d_{001}=14.72 Å , Beghout et al.[11].

Table SI-3. Cell optimized parameters for a smectite model with two interlayer Ca cations, $(Al_4Si_8O_{22})_2(OH)_4Ca_2(H_2O)_5(CO_2)_3$-$H_2O$:$SO_2$ or -H_2SO_3.

Model system	*a*	*b*	*c*	*α*	*β*	*γ*	V(Å^3)	d_{001}
H_2O:SO_2	10.46	9.03	12.98	91.2	100.3	89.6	1205.86	12.76
H_2SO_3	10.46	9.04	13.09	91.4	100.7	89.5	1215.00	12.86

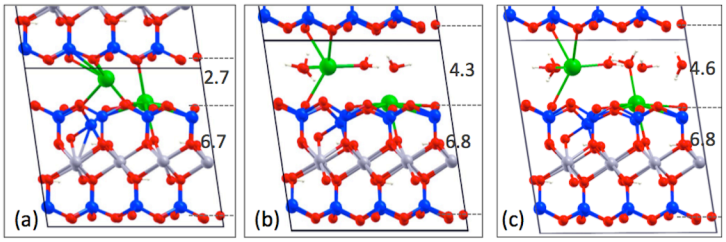

Figure SI-1. Cell-optimized geometries for the (a) 'dry', (b) $4H_2O$, and (c) $6H_2O$ Ca-saturated smectite system.

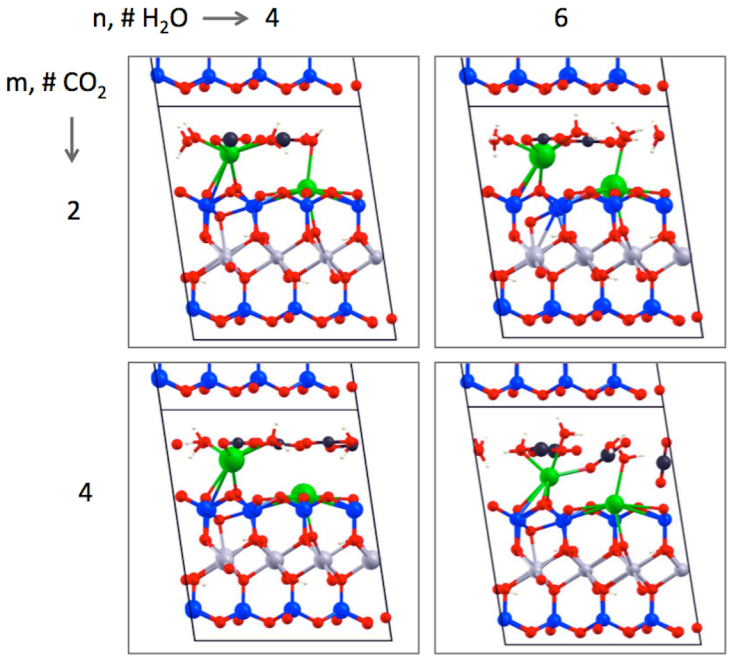

Figure SI-2. Cell-optimized geometries after CO_2 intercalation into the hydrated systems with *n*=4, 6 H_2O and *m*=2, 4 CO_2 molecules.

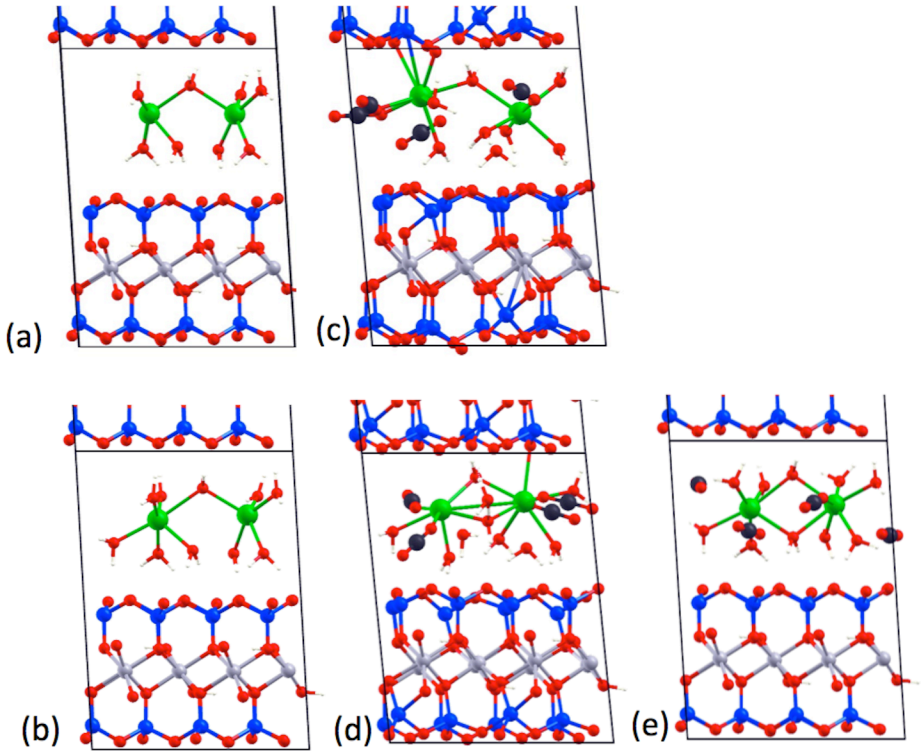

Figure SI-3. Cell optimized structures with (a) 8 waters, (b) 10 waters, (c) quasi-monolayer with $8H_2O/4\ CO_2$, (d) quasi-monolayer with $10H_2O/4CO_2$ and (e) bilayer with $10H_2O/4CO_2$.

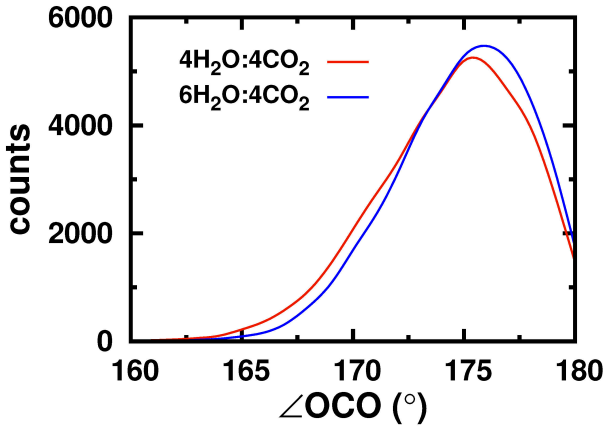

Figure SI-4. Angle distribution of intercalated CO_2 molecules.

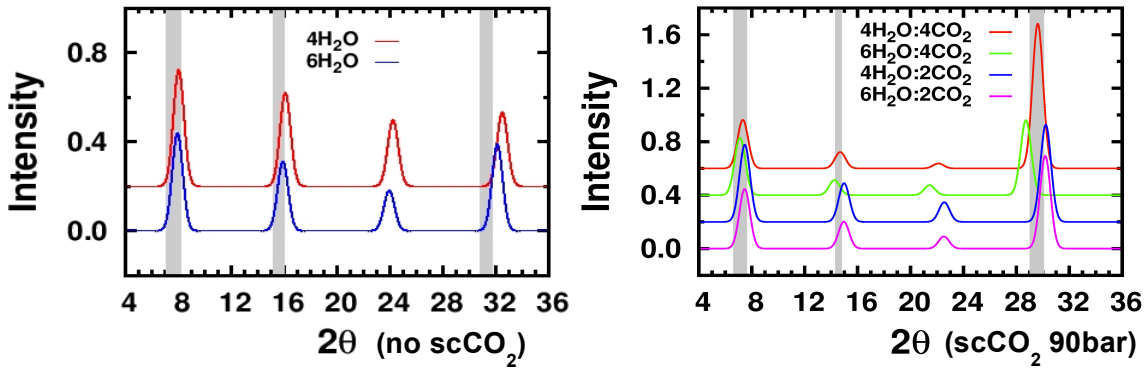

Figure SI-5. Computed XRD pattern for the ~1W Ca-smectite systems, before (left) and after (right) CO_2 intercalation. Shaded regions show the experimental values from Schaef et al.[12]

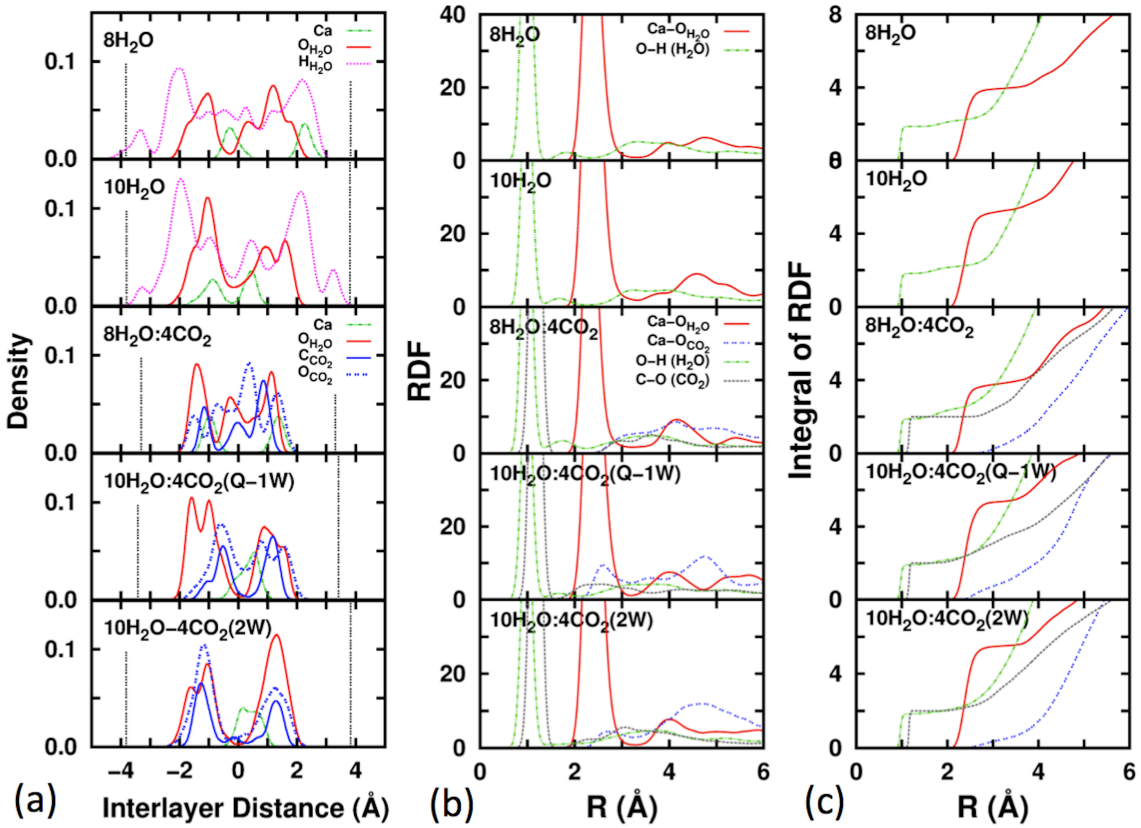

Figure SI-6. (a) Interlayer atomic distributions, (b) radial distribution functions, and (c) integration of the RDFs providing average contacts for Ca-rich montmorillonite in 1W-2W hydration states before and after CO_2 intercalation. RDF showing Ca contact is given as average values of both Ca cations in these systems.

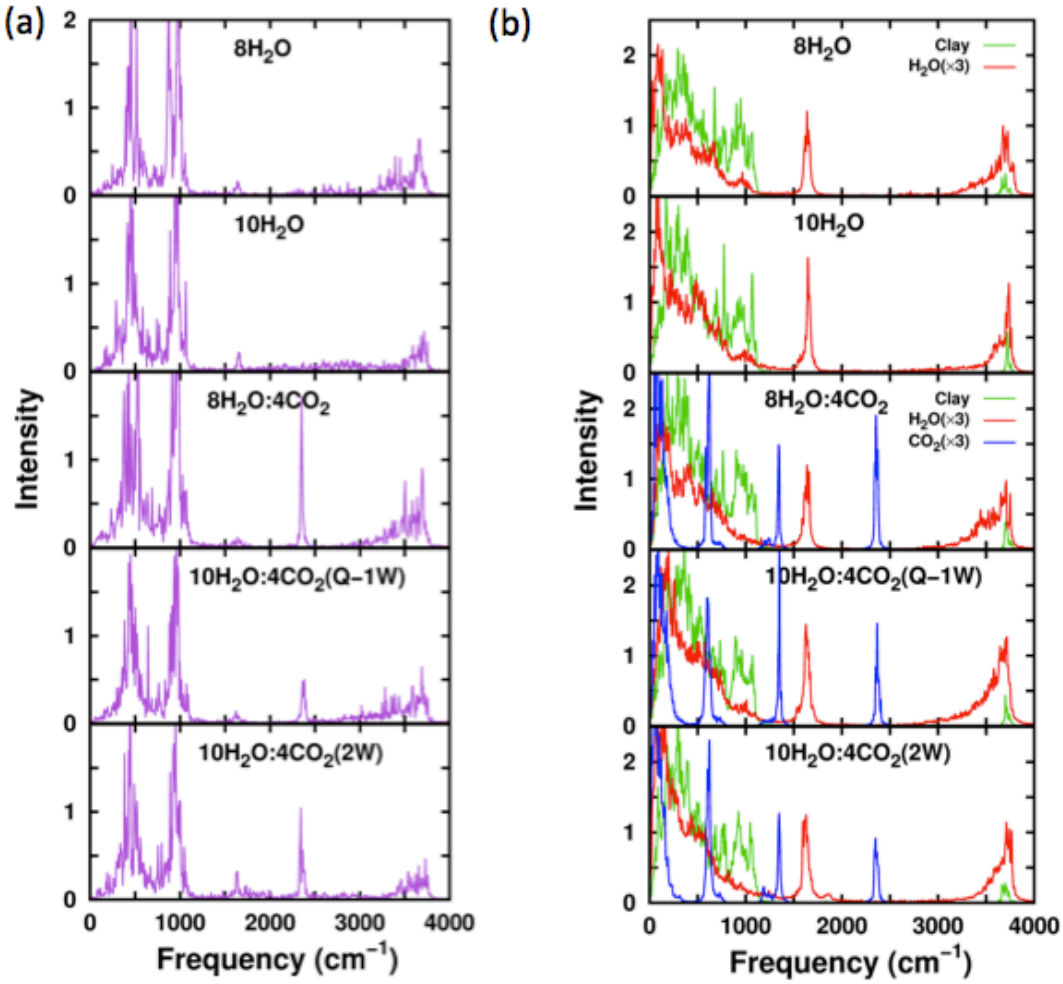

Figure SI-7. (a) IR spectrum from the autocorrelation of the total dipole moment, (b) projected VDOS for the smectite systems with 8 and 10H_2O (top two panels) and after the addition of CO_2 (bottom three panels). 8H_2O:4CO_2 corresponds to 2:1 ratio between H_2O and CO_2 and 2.5:1 ratio for 10H_2O:4CO_2. Q-1W denotes quasi-one water layer structure and 2W denotes two water layer system. Intensities of H_2O and CO_2 are multiplied by 3 for clarification.

References

1. Perdew, J. P.; Burke, K.; Ernzerhof, M., Generalized gradient approximation made simple *Physical Review Letters* **1996,** *77*, 3865.
2. CP2K is a program to perform atomistic and molecular simulations of solid state, liquid, molecular, and biological systems. CP2K is available at http://www.cp2k.org/.
3. VandeVondele, J.; Krack, M.; Mohamed, F.; Parrinello, M.; Chassaing, T.; Hutter, J., QUICKSTEP: Fast and accurate density functional calculations using a mixed Gaussian and plane waves approach *Computer Physics Communications* **2005,** *167*, 103.
4. Grimme, S.; Hujo, W.; Kirchner, B., Performance of dispersion-corrected density functional theory for the interactions in ionic liquids *Physical Chemistry Chemical Physics* **2012,** *14*, 4875.
5. Ehrlich, S.; Moellmann, J.; Reckien, W.; Bredow, T.; Grimme, S., Sytem-dependent dispersion coefficients for the DFT-D3 treatment of adsoprtion processes on ionic surfaces. *ChemPhysChem* **2011,** *12*, 3414.
6. Goedecker, S.; Teter, M.; Hutter, J., Separable dual-space Gaussian pseudopotentials *Physical Review B* **1996,** *54*, 1703.
7. Krack, M., Pseudopotentials for H to Kr optimized for gradient-corrected exchange-correlation functionals *Theoretical Chemistry Accounts* **2005,** *114*, 145.
8. VandeVondele, J.; Hutter, J., Gaussian basis sets for accurate calculations on molecular systems in gas and condensed phases *J. Chem. Phys.* **2007,** *127*, 114105.
9. Lippert, G.; Hutter, J.; Parrinello, M., A hybrid Gaussian and plane wave density functional scheme *Molecular Physics* **1997,** *92*, 477.
10. Viani, A.; Gaultieri, A. F.; Artioli, G., The nature of disorder in montmorillonite by simulation of X-ray powder patterns *American Mineralogist* **2002,** *87*, 966.
11. Berghout, A.; Tunega, D.; Zaoui, A., Density Functional Theory (Dft) Study Of The Hydration Steps Of Na^{+}/Mg^{2+}/Ca^{2+}/Sr^{2+}/Ba^{2+}-Exchanged Montmorillonites *Clays and Clay Minerals* **2010,** *58*, 174.
12. Schaef, H. T.; Ilton, E. S.; Qafoku, O.; Martin, P. F.; Felmy, A. R.; Rosso, K. M., In situ XRD study of Ca2+ saturated montmorillonite (STX-1) exposed to anhydrous and wet supercritical carbon dioxide *International Journal of Greenhouse Gas Control* **2012,** *6*, 220.
13. Liang, Y.; Miranda, C. R.; Scandolo, S., Temperature-induced densification of compressed SiO2 glass: A molecular dynamics study *High Pressure Research* **2008,** *28*, 35.
14. Brown, P. J.; Fox, A. G.; Maslen, E. N.; O'Keefe, M. A.; Willis, B. T. M., International Tables for Crystallography, Chapter 6.1. 2006; Vol. C, pp 554-595.
15. Ramírez, R.; López-Ciudad, T.; Kumar, P.; Marx, D., Quantum corrections to classical time-correlation functions: Hydrogen bonding and anharmonic floppy modes. *The journal of Chemical Physics* **2004,** *121*, 3973.
16. Silvestrelli, P. L.; Bernasconi, M.; Parrinello, M., Ab initio infrared spectrum of liquid water *Chemical Physics Letters* **1997,** *277*, 478.
17. Ndongmouo, U. F. T.; Lee, M.-S.; Rousseau, R.; Baletto, F.; Scandolo, S., Finite-Temperature Effects on the Stability and Infrared Spectra of HCl (H2O) 6 Clusters *The Journal of Physical Chemistry A* **2007,** *111*, 12810.

18. De Sousa, R. L.; Leite Alves, H. W., *Brazilian Journal of Physics* **2005,** *36*, 501.
19. Abramova, E.; Lapides, I.; Yariv, S., Thermo-XRD investigation of monoionic montmorillonites mechanochemically treated with urea *Journal of Thermal Analysis and Calorimetry* **2007,** *90*, 99.
20. Bray, H. J.; Redfern, S. A. T., Kinetics of dehydration of Ca-montmorillonite *Physics and Chemistry of Minerals* **1999,** *26*, 591.
21. Cases, J. M.; Berend, I.; Francois, M.; Uriot, J. P.; Michot, L. J.; Thomas, F., Mechanism of adsorption and desorption of water vapor by homoionic montmorillonite .3. The Mg2+, Ca2+, Sr2+ and Ba2+ exchanged forms *Clays and Clay Minerals* **1997,** *45*, 8.
22. Ferrage, E.; Lanson, B.; Sakharov, B. A.; Drits, V. A., Investigation of smectite hydration properties by modeling experimental X-ray diffraction patterns: Part I. Montmorillonite hydration properties *American Mineralogist* **2005,** *90*, 1358.
23. Rutherford, D. W.; Chiou, C. T.; Eberl, D. D., Effects of exchanged cation on the microporosity of montmorillonite *Clays and Clay Minerals* **1997,** *45*, 534.
24. Sato, T.; Watanabe, T.; Otsuka, R., Effects Of Layer Charge, Charge Location, And Energy Change On Expansion Properties Of Dioctahedral Smectites *Clays and Clay Minerals* **1992,** *40*, 103.
25. Chatterjee, A.; Ebina, T.; Onodera, Y.; Mizukami, F., Effect of exchangeable cation on the swelling property of 2 : 1 dioctahedral smectite - A periodic first principle study *Journal of Chemical Physics* **2004,** *120*, 3414.